Journal of Power Sources 196 (2011) 4128–4135

Contents lists available at ScienceDirect

Journal of Power Sources

journal homepage: www.elsevier.com/locate/jpowsour

# Modeling and characterization of supercapacitors for wireless sensor network applications

Ying Zhang*, Hengzhao Yang

*School of Electrical and Computer Engineering, Georgia Institute of Technology, Atlanta, GA 30332, USA*

ARTICLE INFO

*Article history:*
Received 4 October 2010
Received in revised form
29 November 2010
Accepted 29 November 2010
Available online 4 December 2010

*Keywords:*
Supercapacitor modeling
Charging
Redistribution
Self-discharge
Wireless sensor networks

ABSTRACT

A simple circuit model is developed to describe supercapacitor behavior, which uses two resistor–capacitor branches with different time constants to characterize the charging and redistribution processes, and a variable leakage resistance to characterize the self-discharge process. The parameter values of a supercapacitor can be determined by a charging-redistribution experiment and a self-discharge experiment. The modeling and characterization procedures are illustrated using a 22F supercapacitor. The accuracy of the model is compared with that of other models often used in power electronics applications. The results show that the proposed model has better accuracy in characterizing the self-discharge process while maintaining similar performance as other models during charging and redistribution processes. Additionally, the proposed model is evaluated in a simplified energy storage system for self-powered wireless sensors. The model performance is compared with that of a commonly used energy recursive equation (ERE) model. The results demonstrate that the proposed model can predict the evolution profile of voltage across the supercapacitor more accurately than the ERE model, and therefore provides a better alternative for supporting research on storage system design and power management for wireless sensor networks.



## 1. Introduction

Harvesting energy from ambient environment to power wireless sensor networks (WSNs) has been investigated to extend system lifetime [1–8]. Rechargeable batteries such as NiMH [1] and Li-ion [2] were first selected to serve as primary energy storage devices. While rechargeable batteries have high capacity and low leakage, the cycle life of rechargeable batteries limits the lifetime of wireless sensors [3,5,6]. The cycle life of a rechargeable battery is defined as the number of charge–discharge cycles before its capacity falls below 80% of its initial rated capacity. The aging process during the charge–discharge cycles results in a gradual reduction in capacity and an increase in internal resistance over time [9]. By the end of the cycle life, the capacity of a rechargeable battery is reduced by 20% and the useful energy drops to 50% because the higher internal resistance causes premature end of life [3]. Due to limited cycle life, typically ranges from 100 s to 1000 s [10], a wireless sensor node will require battery replacement after 1–2 years [3,5,6]. Compared with rechargeable batteries, supercapacitors have a much longer cycle life and higher charge–discharge efficiency in addition to fast charge–discharge characteristic [3,5–7,11,12]. Some authors have proposed to use supercapacitors alone to store harvested energy [3,12] or use supercapacitors in combination with rechargeable batteries [5–7,11] to achieve "perpetual lifetimes" for wireless sensor networks.

Due to wide range of potential applications of self-powered WSNs, there is considerable research interest in developing efficient power storage systems [11,12], power management algorithms [13] and communication protocols [14]. A supercapacitor model is an important tool for evaluating these researches using analytical methods or simulation before being demonstrated in practical deployments. Currently adopted supercapacitor models in WSN research are developed from the supercapacitor leakage power profiles [5,11,12,14,15], which are called the energy recursive equation (ERE) models in this paper. The ERE model assumes the capacitance of a supercapacitor is constant, and uses a long-term leakage power profile to determine leakage at any time [12]. However, the physics of the supercapacitor suggests that its capacitance depends on the terminal voltage across the device and the supercapacitor usually experiences internal charge redistribution during and after charge and discharge cycles [16]. Without capturing these properties, the terminal voltage estimated using the ERE model may have significant deviation from the actual value. The voltage deviation can cause improper decision making in a power management system for self-powered wireless sensors that harvest ambient energy and experience frequent charge–discharge cycles. The improper decision may even lead to failure of a wireless sensor network.

* Corresponding author. Tel.: +1 912 963 2572; fax: +1 912 966 7928.
*E-mail address:* yzhang@gatech.edu (Y. Zhang).

0378-7753/$ – see front matter © 2010 Elsevier B.V. All rights reserved.
doi:10.1016/j.jpowsour.2010.11.152

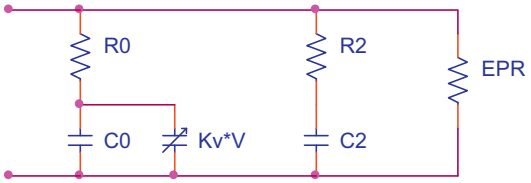


**Fig. 1.** Two-branch model with EPR [31].

A simple equivalent circuit model for supercapacitors that can accurately model charging, redistribution and self-discharge processes is presented in this paper. A supercapacitor with rated capacitance of tens Farads, typical capacity for WSN applications, is used as an example to illustrate the modeling and characterization process. The performance of the developed model is compared with that of models used in power electronics applications that often target supercapacitors with rated capacitances of kilo-Farads. In addition, the developed model is compared with the ERE model in analyzing a simplified energy storage system for wireless sensors. The results demonstrate that the new model provides a more accurate estimation of terminal voltages across the supercapacitor than the currently used ERE model and hence a better alternative for supporting research on storage system design and power management in WSNs.

## 2. Modeling and characterization of supercapacitors

The electrochemical impedance spectroscopy (EIS) is a general approach to measure the complex impedance of energy storage devices such as supercapacitors and batteries [17]. The nature of impedances in various frequency ranges can be determined by analyzing the frequency dependencies of the real part and the imaginary part [18]. Various equivalent circuit models [19,20] have been developed using the porous electrode theory [21–26] to interpret the impedance spectrum of a supercapacitor. With the assumption of homogeneous electrode pore size, a general porous impedance model consists of three impedances linking to electrode, electrolyte and electrode/electrolyte interface [23–25]. The general model can be modified if interface roughness [27] or random pore size [28] is considered. The impedance spectrum can be modeled by N interleaved RC circuits which would require the calculation of 2N parameters [17]. However, it is usually very hard to determine more than five or six independent parameters efficiently due to the strong influences between them [17].

Alternatively, supercapacitors can be characterized in time domain by conducting various experiments such as constant power tests and constant current tests [18]. In power electronics applications, this approach is often used to develop an equivalent circuit to model the terminal behavior of supercapacitors [16,29]. As supercapacitors are usually constructed with two porous carbon electrodes impregnated with electrolyte and separated by a porous insulating membrane, the interface electrochemistry suggests a complex network of non-linear capacitors connected between them by resistances can describe the behavior of supercapacitors [29]. In the network, resistors represent the resistivity of carbon particles and capacitors describe the capacitance between carbon and electrolyte [16]. In practical applications, simplified versions are required to enable model implementation [29]. One often used version is the two-branch model [31] shown in Fig. 1. The first branch is the main branch, which includes $R_0$ and the voltage dependent capacitance ($C_0$ and $K_vV$). The main branch, also called the immediate branch, dominates the immediate behavior of a supercapacitor in response to a charge action and captures the linear dependence of capacitance on the terminal voltage in the practical voltage range of the device [16]. This branch determines short-term voltage evolution during charge and discharge cycles [16,31], The second branch ($R_2$ and $C_2$) is the delayed branch, which represents the medium and long term charge redistribution [16,31]. The voltage relaxation is the result of charge redistribution [32]. The equivalent parallel resistance (EPR) represents the effect of self-discharge [16,31].

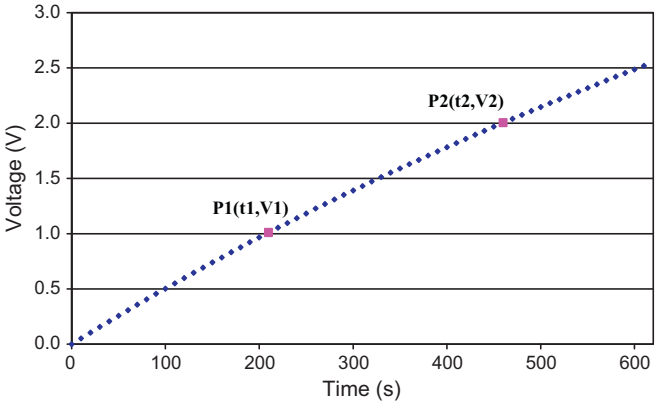


**Fig. 2.** A 22F supercapacitor charged with a constant 97 mA current.

### 2.1. $R_0$

The resistance $R_0$ can be determined by measuring the potential difference $\Delta V$ between the two terminals at the beginning while charging the supercapacitor with a large constant charging current $I_C$ [16,31]. The ratio of initial short-term potential change and $I_C$ determines the $R_0$ value. As the $R_0$ value identified using this approach is very close to the ESR (equivalent series resistance) value provided by the supercapacitor datasheet, it is reasonable to use ESR value for $R_0$.

### 2.2. $C_0$ and $K_v$

Assuming all the charge is stored in the first branch during the charging process, the current–voltage relationship across the capacitor of the first branch is [31]:

$$i = \frac{dq}{dt} = \frac{dq}{dv}\frac{dv}{dt} = (C_0 + K_V v)\frac{dv}{dt} \tag{1}$$

In case of a constant charging current $I_C$, the time–voltage relationship at the supercapacitor terminals can be derived from (1) as follows:

$$t = f(V) = \frac{C_0}{I_C}V + \frac{1}{2}\frac{K_V}{I_C}V^2 \tag{2}$$

Given two data points $(t_1,V_1)$ and $(t_2,V_2)$ in the time–voltage charging curve with a constant charging current (Fig. 2), the following equations must hold:

$$\begin{cases} t_1 = \dfrac{C_0}{I_C}V_1 + \dfrac{1}{2}\dfrac{K_V}{I_C}V_1^2 \\ t_2 = \dfrac{C_0}{I_C}V_2 + \dfrac{1}{2}\dfrac{K_V}{I_C}V_2^2 \end{cases} \tag{3}$$

The values for $C_0$ and $K_v$ can be solved from (3):

$$\begin{cases} C_0 = \left[\dfrac{t_1}{V_1} - \dfrac{V_1t_2 - t_1V_2}{V_2^2 - V_1V_2}\right] I_C \\ K_V = 2\left[\dfrac{V_1t_2 - t_1V_2}{V_1V_2^2 - V_1^2V_2}\right] I_C \end{cases} \tag{4}$$

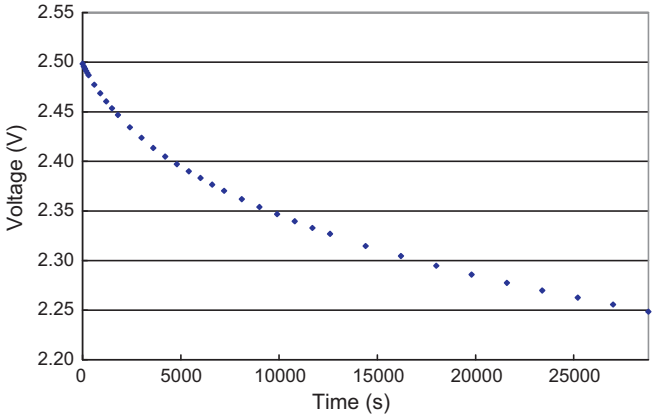


**Fig. 3.** Self-discharge of a fully charged 22F supercapacitor.

### 2.3. $C_2$ and $R_2$

After the supercapacitor reaches its rated voltage, the charging current is removed. The charge stored in the first branch charges the second branch during the redistribution process [31]. If the time constant of the second branch $\tau_2 = R_2C_2$ is fixed, we can assume the voltages of both branches are same at time $3\tau_2$. The value $\tau_2 = 240$ s can be used as a starting point [31]. If it does not provide sufficient accuracy for the model, more experimental tests can be performed to adjust the value. Once the time constant of the second branch is determined, the voltage of the supercapacitor at time $3\tau_2$, $V_{2f}$, during the redistribution process can be measured. At this point, assuming all charge is stored in the supercapacitor, $C_2$ can be determined from the following equation:

$$Q_{tot} = I_C T_C = C_2 V_{2f} + \left(C_0 + \frac{K_V}{2} V_{2f}\right) V_{2f} \quad (5)$$

where $T_C$ is the charging time. Then the value of resistor $R_2$ is:

$$R_2 = \frac{\tau_2}{C_2} \quad (6)$$

## 3. Modeling supercapacitor self-discharge

A charged supercapacitor is in a state of higher Gibbs energy than in its discharged state [33]. Therefore a thermodynamic "driving force" results in spontaneous decline of Gibbs energy [33]. This decline manifested as decay in supercapacitor voltage is the self-discharge. The rate of self-discharge, which usually diminishes with time, actually determines the shelf-life of supercapacitors [34]. Fig. 3 shows the self-discharge of a 22F supercapacitor. The open circuit voltage of the supercapacitor is measured for 8 h after it is fully charged to its rated voltage 2.5 V with a constant voltage source. It is obvious that the self-discharge rate decreases with time.

The open-circuit self-discharge of supecapacitors must take place through coupled anodic and cathodic processes to pass parasitic currents at one or both individual electrodes since there is no external circuit through which discharge can pass [33]. The self-discharge can be ascribed to three mechanisms [30,34,35]: activation-controlled Faradaic processes if the supercapacitor is overcharged, diffusion-controlled Faradaic redox reactions if the supercapacitor is not overcharged but some depolarizing impurity is present, and leakage current if the supercapacitor has internal ohmic leakage pathways. Under the normal operation conditions, both diffusion-controlled Faradaic redox reactions and internal ohmic leakage need to be modeled.

The two-branch model, in which the self-discharge is represented with a constant equivalent parallel resistance (EPR), only considers the internal ohmic leakage. To model the nonlinear self-discharge, Diab et al. [36] proposed a three-branch model (Fig. 4) in which the $R_rC_r$ branch was added to represent the self-discharge due to diffusion-controlled Faradic redox reactions.

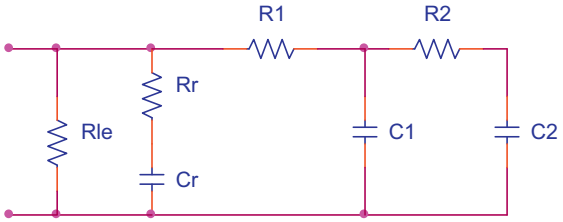


**Fig. 4.** Three-branch model [36].

The leakage current due to diffusion-controlled Faradic redox reactions is proportional to the concentration gradient of the diffusible redox species. The time-dependence of the concentration gradient at a particular distance from a plane electrode is generally inversely proportional to the square-root of time, which leads to a decrease of self-discharge rate with time [34]. We propose to use a variable leakage resistance (VLR) to model the time dependency of self-discharge (Fig. 5). We do not distinguish different self-discharge mechanisms. Rather, we introduce a single VLR to take into account the effects of various self-discharge mechanisms under the normal operation conditions.

With a constant leakage resistance EPR (Fig. 1), the self-discharge can be described by the following exponential function [36]:

$$v(t) = V_0 \exp\left(-\frac{t}{\tau_{le}}\right) \quad (7)$$

where $V_0$ is the initial voltage and $\tau_{le}$ is the time constant of leakage current.

Once the time constant of leakage current is determined experimentally, the leakage resistance EPR can be calculated based on the following equation [36]:

$$\text{EPR} = \frac{\tau_{le}}{C_1} \quad (8)$$

with a variable leakage resistance, VLR, instead of using one exponential function to model the self-discharge characteristic, we use several distinct exponential functions. These exponential functions have different time constants during different self-discharge periods, which result in different leakage resistances. By trial and error, we found that five distinct exponential functions (Eq. (9)) corresponding to five periods can fit the self-discharge measurement of a supercapacitor up to 28,800 s (8 h) very well (Fig. 6(a)). Fig. 6(b) shows a zoomed-in result for the self-discharge during the first 2 h. For the following sections, the self-discharge characteristic will be restricted to the first 2 h because we are more interested in

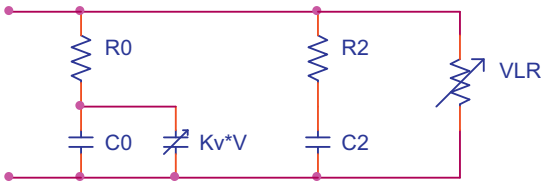


**Fig. 5.** Proposed variable leakage resistance (VLR) model.

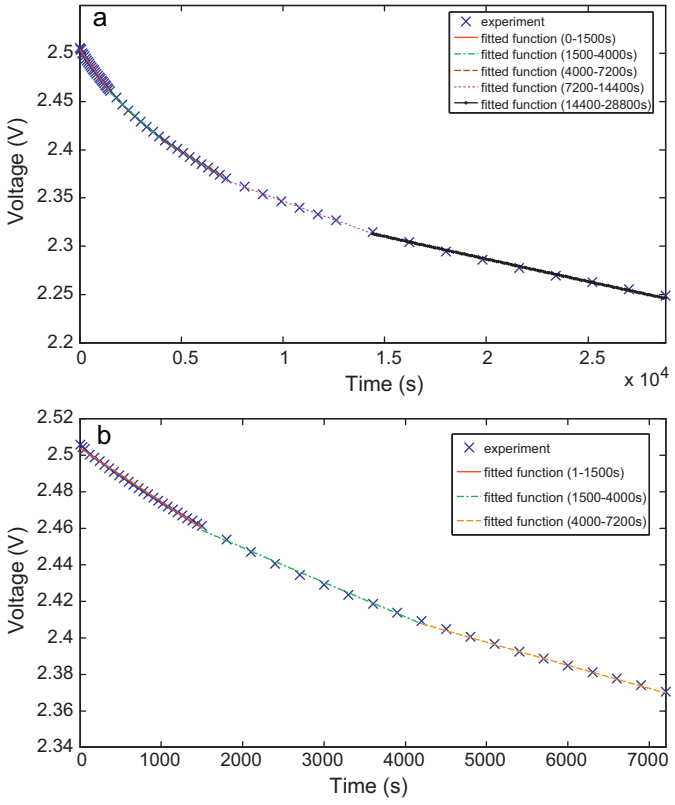


**Fig. 6.** Comparisons between self-discharge measurements and fitted multiple exponential functions: (a) 8 h and (b) 2 h.

the short and medium term behavior of supercapacitors.

$$v(t) = \begin{cases} 2.504\ \exp(-1.181 \times 10^{-5} t), & t = (0, 1500\ \text{s}) \\ 2.488\ \exp(-7.807 \times 10^{-6} t), & t = (1500, 4000\ \text{s}) \\ 2.462\ \exp(-5.301 \times 10^{-6} t), & t = (4000, 7200\ \text{s}) \\ 2.425\ \exp(-3.279 \times 10^{-6} t), & t = (7200, 14400\ \text{s}) \\ 2.382\ \exp(-2.042 \times 10^{-6} t), & t = (14400, 28800\ \text{s}) \end{cases} \quad (9)$$

## 4. Evaluation of the VLR model

The VLR model for a 22F supercapacitor from Cooper Bussmann [37] was developed following the characterization process described in Sections 2 and 3. The charging, redistribution and self-discharge processes were performed for identifying model parameter values. During the charging and redistribution processes, the initially completely discharged supercapacitor was charged for 610 s using a constant current source (97 mA). Then the current source was turned off and the decline of voltage across the supercapacitor due to redistribution was tallied for the next 890 s. During the self-discharge process, we assumed that the supercapacitor was fully charged after being charged for 1 h with a 2.5 V constant voltage source. The self-discharge was recorded for 2 h after removing the voltage source.

To reduce random measurement errors, each experiment was repeated three times to obtain an average. Fig. 7 shows the experimental data and the corresponding average values. The root mean

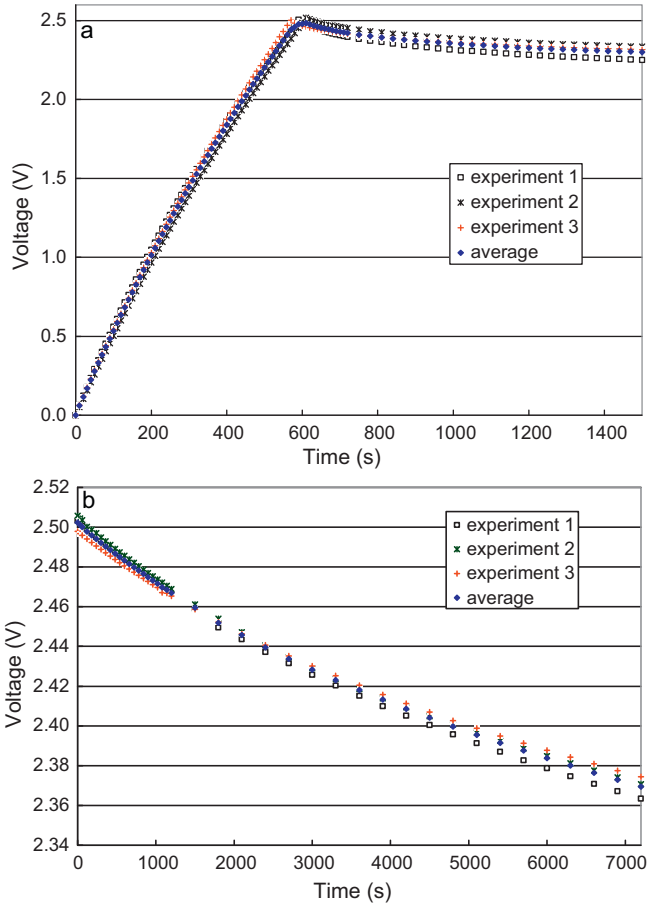


**Fig. 7.** Comparisons between three experiments: (a) charging and redistribution processes and (b) self-discharge process.

square error (RMSE) between the measured experimental data and the average is below 0.05 V for the charging and redistribution processes (Fig. 7(a)), and below 0.005 V for the self-discharge process (Fig. 7(b)). The RMSEs are relatively small compared to the voltage ranges involved in the experiments. The model parameter values of the 22F supercapacitor (Table 1) were determined based on the average data. The simulation results of the model match the average of measurements very well for charging, redistribution and self-discharge processes as shown in Fig. 8.

Performance of the proposed VLR model is compared with that of two-branch and three-branch models. The constant leakage resistance EPR in a two-branch model can be determined using the ratio of the nominal voltage and the leakage current reported in the datasheet [31]. For the 22F test sample, the leakage current is not specified in the manufacturer datasheet [37]. To estimate the EPR, we used an exponential function to fit the self-discharge curve [36] and found a leakage resistance value for EPR (4350 Ω) based on Eqs. (7) and (8). A larger value (9000 Ω) and a smaller value (2000 Ω) were also used for comparison.

The comparison of different models is shown in Fig. 9. All models have almost the same performance during the charging process (Fig. 9(a)), and can accurately predict the voltage values across

**Table 1**
VLR model parameters of a 22F supercapacitor from Cooper Bussmann.

| Model parameter | $C_0$ | $K_v$ | $R_0$ [37] | $C_2$ | $R_2$ | Variable leakage resistance (VLR) | | |
|---|---|---|---|---|---|---|---|---|
| | | | | | | 0–1500 s | 1500–4000 s | 4000–7200 s |
| Value | 16.2F | 4.8F/V | 0.04 Ω | 2.3F | 210 Ω | 2956 Ω | 4398 Ω | 6523 Ω |

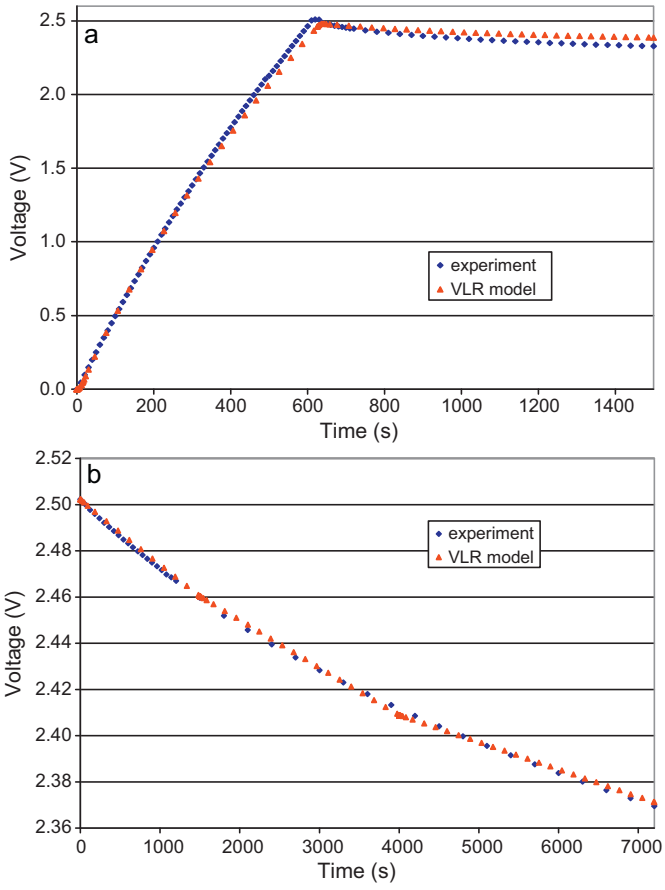


**Fig. 8.** Comparisons between the experiment and the simulation results of VLR model: (a) charging and redistribution processes and (b) self-discharge process.

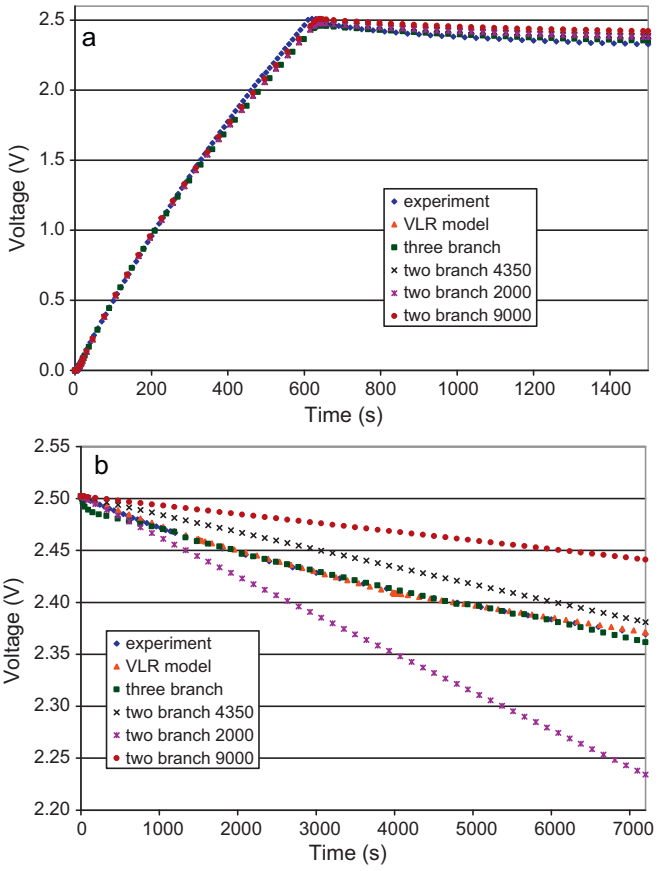


**Fig. 9.** Comparisons between different models of supercapacitors: (a) charging and redistribution processes and (b) self-discharge process.

the supercapactior during the linear charging region. At the end of the charging process, the voltage value is slightly underestimated by all models. During the redistribution process (Fig. 9(a)), three-branch model has the best performance, but other models also have fairly accurate prediction except the two-branch model with EPR of 9000 Ω. During the self-discharge process (Fig. 9(b)), the VLR model has much better performance than other models and its simulation results almost overlap the experimental data. The prediction of the three-branch model has noticeable discrepancies from the measurements. The simulation results are smaller than the measurements during the initial and ending phases of the simulation, and slightly larger during the middle period. The two-branch model with three different EPRs behaves poorly during the measured self-discharge period.

## 5. Comparison of the VLR and ERE models in self-powered wireless sensor networks

Supercapacitors have been used as alternative energy storage devices for self-powered wireless sensor networks [3,5,12] due to their long charge–discharge cycle lives. Accurate supercapacitor models are critical for designing efficient energy storage systems and supporting power management related research. The current commonly used models, ERE models, are based on leakage characteristics of supercapacitors [5,12]. In this section, performance of the VLR model is compared with that of the ERE model in a simplified self-powered sensor node.

### 5.1. Energy recursive equation (ERE) model

The ERE model is developed based on the leakage power profile of the supercapacitor. After a supercapacitor is fully charged, the voltage between two terminals of the supercapacitor, V, is measured during the leakage process. The residual energy stored in the supercapacitor can be calculated from the voltage at different sampling time and rated capacitance [5,15].

$$E_{\text{residual}} = \frac{1}{2}CV^2 \tag{10}$$

Then the energy leaked over a period of time can be calculated. The leakage power can be further derived by dividing the leaked energy by the sampling period [15].

The leakage power profile of the 22F supercapacitor from Cooper Bussmann for 2 h is shown in Fig. 10. The leakage power profile

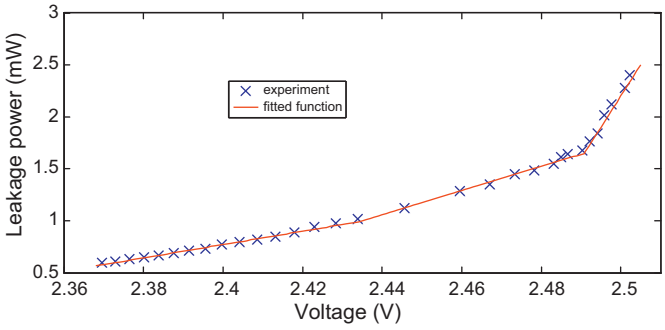


**Fig. 10.** Leakage power profile of a 22F supercapacitor.

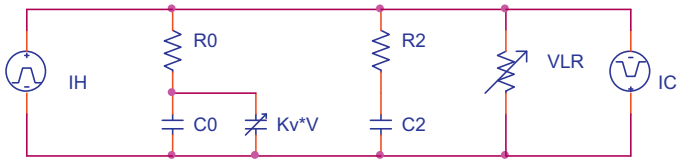


**Fig. 11.** Evaluation setup for supercapacitor storage systems.

can be approximated with the following piecewise linear function [12,15].

$$P_{\text{leakage}} = \begin{cases} 60.2V - 148.3, & V = (2.491\text{–}2.505\ \text{V}) \\ 12.61V - 27.27, & V = (2.434\text{–}2.491\ \text{V}) \\ 6.417V - 14.63, & V = (2.368\text{–}2.434\ \text{V}) \end{cases} \quad (11)$$

Taking the harvested energy and consumed energy into account, the energy stored in the supercapacitor at the end of every T-second slot is [12]:

$$E(n+1) = E(n) + E_{\text{harvested}}(n) - E_{\text{consumed}}(n) - P_{\text{leakage}}(n) \times T \quad (12)$$

where $E(n+1)$ and $E(n)$ are the residual energies at the beginning of the $(n+1)$th and $n$th time slots, $E_{\text{harvested}}(n)$ and $E_{\text{consumed}}(n)$ are the harvested and consumed energy during the $n$th time slot, $P_{\text{leakage}}(n)$ is the leakage power corresponding to $E(n)$ and is treated as a constant during the fixed short time slot $T$. The supercapacitor voltage can be calculated from the residual energy [5].

$$V(n+1) = \sqrt{\frac{2E(n+1)}{C}} \quad (13)$$

### 5.2. Experiment setup

A simplified energy storage system with a harvester and a consumer is shown in Fig. 11 assuming the VLR model is used for the supercapacitor. If the ERE model is used, we resort to the energy recursive equations (Eqs. (11)–(13)) to calculate the supercapacitor voltage. The energy harvester (such as a solar panel) is modeled as a constant current source IH [7] with variable magnitude and duty cycle, which charges the supercapacitor when it is turned on. The energy consumer (for example, a Telos mote [8]) is also modeled as a constant current source IC. It drains current from the energy storage system. To examine performance of the two supercapacitor models, the energy storage system is limited to a single supercapacitor (the 22F supercapacitor used to illustrate characterization process) without considering the input and output regulators.

The energy harvester and consumer current profiles are shown in Fig. 12. The supercapacitor was completely discharged at the beginning of simulation. Then the harvester (200 mA) was turned on for 270 s, which charged the supercapacitor close to its rated voltage 2.5 V. The supercapacitor was subject to redistribution in

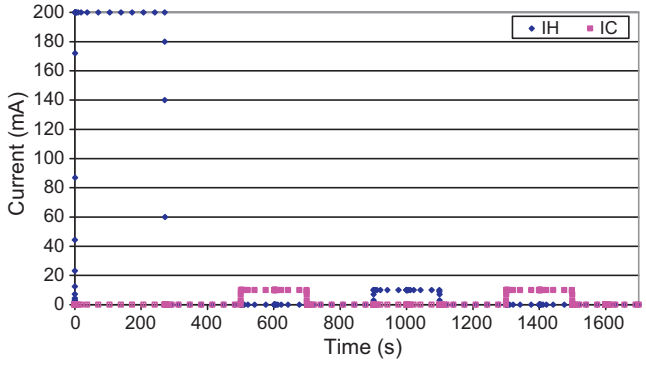


**Fig. 12.** Energy harvester and consumer profiles.

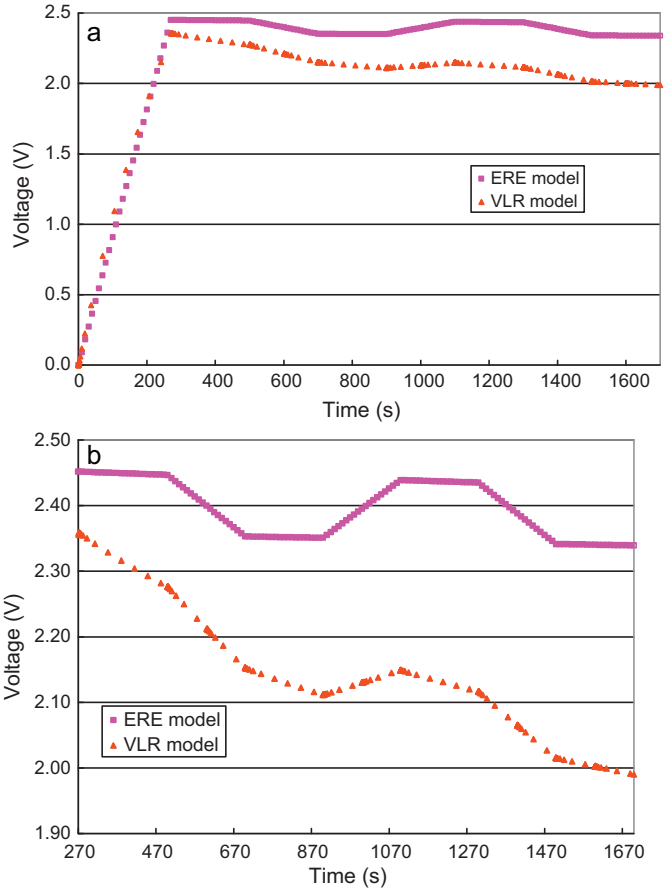


**Fig. 13.** Comparisons between simulation results of VLR and ERE models: (a) simulation results during 0–1700 s and (b) simulation results during 270–1700 s.

the following 230 s. From 500 to 700 s, the consumer was activated and drained a constant current of 10 mA. The system was idle and the supercapacitor experienced self-discharge in the next 200 s. Then another harvester current pulse (10 mA) charged the supercapacitor from 900 to 1100 s to replenish the storage device. After that, the supercapacitor repeated redistribution, discharging and self-discharge in the following 600 s.

### 5.3. Results and discussion

The supercapacitor voltage evolution profiles simulated using VLR and ERE models during the 1700 s are shown in Fig. 13(a). Fig. 13(b) zooms in the results for 270–1700 s. In the first charging period (0–270 s) in Fig. 13(a), the voltages predicted by two models are similar except at the end of this charging period. The voltage value predicted by the ERE model is 0.0959 V more than that of the VLR model at 270 seconds. The voltage difference between VLR and ERE models then increases with time (Fig. 13(b)). The voltage drop predicted by the ERE model (0.0050 V) is much smaller than that of the VLR model (0.0821 V) during the first redistribution period (270–500 s). This is because the VLR model considers the internal charge redistribution while the ERE model does not. For the VLR model, during the charging process, not all internal capacitances are charged to the same voltage level. Part of the charge stored in the first branch is redistributed to the second branch after the charging current is turned off, which reduces the voltage value between two terminals of the supercapacitor. This was called "voltage relaxation" in [32]. The small voltage drop predicted by the ERE model during this period is the result of self-discharge, which is also considered in the VLR model.

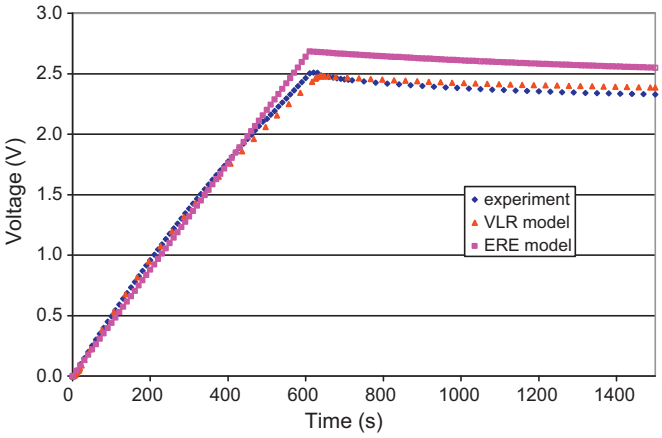


**Fig. 14.** Comparison between experiment and simulation results of VLR and ERE models during the charging and redistribution processes.

The accuracy of these two models during the charging and redistribution processes can be evaluated using experimental data from Fig. 8(a). The simulation setup emulated the experiment. The consumer current source was turned off. During the charging and redistribution processes, the supercapacitor was first completely discharged, and then the energy harvester was turned on with a constant current of 97 mA for 610 s (charging process) and turned off for the next 890 s (redistribution process). The comparison of results (Fig. 14) shows that the VLR model can more accurately predict the experimental data than the ERE model during the charging and redistribution processes. The supercapacitor voltage at the end of the charging process was overestimated by the ERE model, which was also carried over to the redistribution process. This explains the higher voltage values predicted by the ERE model in Fig. 13.

In the discharging period (500–700 s), the current drained by the consumer was much larger than redistribution and self-discharge rates. The voltage drop shown in Fig. 13 is mainly the result of the discharge current. The difference between the voltage drops for the two models (0.0949 V for ERE model and 0.1241 V for VLR model) is still contributed from the redistribution modeled by the VLR model. In the next idle period (700–900 s), redistribution again results in a larger voltage drop for the VLR model (0.0408 V) compared with the ERE model (0.0021 V). For the second phase of simulation (900–1700 s), the voltage differences between two models follow the same pattern. A significant voltage difference (0.3488 V) is resulted at the end of the experiment (1700 s). The voltage difference between two models in Fig. 13 is mainly the results of the internal charge redistribution. Since a supercapacitor in a self-powered sensor node experiences frequent charging, redistribution and discharging cycles, the voltage difference will further increase if the simulation period is extended.

## 6. Conclusions

An equivalent circuit model of supercapacitors is proposed and the characterization process is illustrated. A variable leakage resistance (VLR) is connected in parallel with two resistor–capacitor branches to model the nonlinearity of supercapacitor self-discharge. The VLR represents both leakage due to diffusion-controlled Faradaic redox reactions, which is a nonlinear process, and internal ohmic leakage. The proposed VLR model increases model accuracy while maintaining simplicity of circuit structure. Performance of the VLR model is compared with that of three-branch and two-branch models. Results show that the VLR model has better accuracy in predicting self-discharge of supercapacitors while offering comparable accuracy for charging and redistribution processes.

The VLR model is also evaluated in a simplified energy storage system for a self-powered wireless sensor node. Performance of the VLR model is compared with that of the ERE (energy recursive equation) supercapacitor model currently used for research in wireless sensor networks. The difference between these two models is due to that the ERE model does not model the supercapacitor internal charge redistribution, which results in overestimation of terminal voltages of supercapacitors. Therefore, the VLR model provides a better alternative tool for supporting research on energy storage system design and power management strategies for self-powered wireless sensor networks.

## References

[1] J. Taneja, J. Jeong, D. Culler, Proceedings of the 7th International Conference on Information Processing in Sensor Networks (IPSN'08), April 22–24, 2008, pp. 407–418.
[2] P. Zhang, C.M. Sadler, S.A. Lyon, M. Martonosi, Proceedings of the 2nd International Conference on Embedded Networked Sensor Systems (SenSys'04), November 3–5, 2004, pp. 227–238.
[3] F. Simjee, P.H. Chou, Proceedings of the 2006 International Symposium on Low Power Electronics and Design (ISLPED'06), October 4–6, 2006, pp. 197–202.
[4] P. Dutta, J. Hui, J. Jeong, S. Kim, C. Sharp, J. Taneja, G. Tolle, K. Whitehouse, D. Culler, Proceedings of the 5th International Conference on Information Processing in Sensor Networks (IPSN'06), April 19–21, 2006, pp. 407–415.
[5] X. Jiang, J. Polsatre, D. Culler, Proceedings of the 4th International Symposium on Information Processing in Sensor Networks (IPSN'05), April 15, 2005, pp. 463–468.
[6] J. Alberola, J. Pelegri, R. Lajara, J.J. Perez, Proceedings of the IEEE Instrumentation and Measurement Technology Conference (I2MTC'08), May 12–15, 2008, pp. 657–662.
[7] J. Jeong, X. Jiang, D. Culler, Proceedings of the 5th International Conference on Networked Sensing Systems (INSS'08), June 17–19, 2008, pp. 181–188.
[8] J. Polastre, R. Szewczyk, D. Culler, Proceedings of the 4th International Symposium on Information Processing in Sensor Networks (IPSN'05), April 15, 2005, pp. 364–369.
[9] T. Umemura, Y. Mizutani, T. Okamoto, T. Taguchi, K. Nakajima, K. Tanaka, Proceedings of the 7th International Conference on Properties and Applications of Dielectric Materials, vol. 3, June 1–5, 2003, pp. 944–948.
[10] GP Batteries Nickel Metal Hydride Technical Handbook, http://www.gpbatteries.com/html/pdf/NiMH_technical.pdf.
[11] H. Yang, Y. Zhang, Proceedings of SPIE, Sensors and Smart Structures Technologies for Civil, Mechanical, and Aerospace Systems 2010, vol. 7647, March 8, 2010, p. 76472U.
[12] T. Zhu, Z. Zhong, Y. Gu, T. He, Z. Zhang, Proceedings of the 7th International Conference on Mobile Systems, Applications, and Services (MobiSys'09), June 22–25, 2009, pp. 319–332.
[13] C. Moser, J. Chen, L. Thiele, Proceedings of the 14th ACM/IEEE International Symposium on Low Power Electronics and Design (ISLPED'09), August 19–21, 2009, pp. 413–418.
[14] A. Kailas, M. Ingram, Y. Zhang, Proceedings of the 1st International Conference on Wireless Communication, Vehicular Technology, Information Theory and Aerospace & Electronic Systems Technology (Wireless VITAE'09), May 17–20, 2009, pp. 42–46.
[15] G. Merrett, A. Weddell, A. Lewis, N. Harris, B. Al-Hashimi, N. White, Proceedings of 17th International Conference on Computer Communications and Networks (ICCCN'08), August 3–7, 2008, pp. 1–6.
[16] L. Zubieta, R. Bonert, IEEE Trans. Ind. Appl. 36 (2000) 199–205.
[17] S. Buller, E. Karden, D. Kok, R.W. De Doncker, IEEE Trans. Ind. Appl. 38 (2002) 1622–1626.
[18] W. Lajnef, J.-M. Vinassa, O. Briat, S. Azzopardi, E. Woirgard, J. Power Sources 168 (2007) 553–560.
[19] F. Rafik, H. Gualous, R. Gallay, A. Crausaz, A. Berthon, J. Power Sources 165 (2007) 928–934.
[20] D. Riu, N. Retiere, D. Linzen, Conference Record of the 2004 IEEE Industry Applications Conference, vol. 4, October 3–7, 2004, pp. 2550–2554.
[21] A.G. Pandolfo, A.F. Hollenkamp, J. Power Sources 157 (2006) 11–27.
[22] A. Celzard, F. Collas, J.F. Marêché, G. Furdin, I. Rey, J. Power Sources 108 (2002) 153–162.
[23] H. Gorh, Electrochem. Appl. 1/97 (1997) 2.
[24] G. Paasch, K. Micka, P. Gersdorf, Electrochim. Acta 38 (1993) 2653–2662.
[25] N. Bertrand, J. Sabatier, O. Briat, J.-M. Vinassa, IEEE Trans. Ind. Electron. 57 (2010) 3991–4000.
[26] E.-H. El Brouji, O. Briat, J.-M. Vinassa, N. Bertrand, E. Woirgard, IEEE Trans. Veh. Technol. 58 (2009) 3917–3929.
[27] G. Sikha, R.E. White, B.N. Popov, J. Electrochem. Soc. 152 (2005) A1682–A1693.
[28] H.-K. Song, H.-Y. Hwang, K.-H. Lee, DaoF L.-H., Electrochim. Acta 45 (2000) 2241–2257.

[29] F. Belhachemi, S. Rael, B. Davat, Conference Record of the 2000 IEEE Industry Applications Conference, vol. 5, October 8–12, 2000, pp. 3069–3076.
[30] B.W. Ricketts, C. Ton-That, J. Power Sources 89 (2000) 64–69.
[31] R. Faranda, Electr. Power Syst. Res. 80 (2010) 363–371.
[32] H. El Brouji, J.-M. Vinassa, O. Briat, N. Bertrand, E. Woirgard, Proceedings of the 2008 IEEE Vehicle Power and Propulsion Conference (VPPC'08), September 3–5, 2008, pp. 1–6.
[33] J. Niu, B.E. Conway, W.G. Pell, J. Power Sources 135 (2004) 332–343.
[34] B.E. Conway, W.G. Pell, T.-C. Liu, J. Power Sources 65 (1997) 53–59.
[35] T.-C. Liu, W.G. Pell, B.E. Conway, Electrochim. Acta 42 (1997) 3541–3552.
[36] Y. Diab, P. Venet, H. Gualous, G. Rojat, IEEE Trans. Power Electron. 24 (2009) 510–517.
[37] Cooper Bussmann PowerStor B Series supercapacitors datasheet, http://www.cooperbussmann.com/pdf/39719066-0619-4987-bc43-55222fa5727a.pdf.